

# Quantification of molecular interactions between ApoE, amyloid-beta (A $\beta$ ) and laminin: Relevance to accumulation of A $\beta$ in Alzheimer's disease

著者	Zekonyte Jurgita, Sakai Kenji, Nicoll James Ar R., Weller Roy O., Carare Roxana O. Ctavia
journal or publication title	Biochimica et Biophysica Acta - Molecular Basis of Disease
volume	1862
number	5
page range	1047-1053
year	2016-05-01
URL	<a href="http://hdl.handle.net/2297/43404">http://hdl.handle.net/2297/43404</a>

doi: 10.1016/j.bbadis.2015.08.025

1 Quantification of molecular interactions between apoE, Amyloid-beta (A $\beta$ ) and laminin:  
2 Relevance to accumulation of A $\beta$  in Alzheimer's disease

3

4 Jurgita Zekonyte<sup>1\*#</sup>, Kenji Sakai<sup>2</sup>, James A. R Nicoll<sup>3</sup>, Roy O Weller<sup>3</sup>, Roxana O Carare<sup>3</sup>

5

6 <sup>1</sup> Faculty of Engineering and Environment, University of Southampton, UK

7 <sup>2</sup> Department of Neurology, Kanazawa University Hospital, Kanazawa, Japan

8 <sup>3</sup> Faculty of Medicine, University of Southampton, UK

9

10

11 \* Corresponding Author

12 Dr. Jurgita Zekonyte

13 School of Engineering

14 University of Portsmouth

15 Anglesea Building, A1.06d

16 Anglesea Road

17 Portsmouth PO1 3DJ

18

19 Tel: +44 (0)23 9284 2330

20 e-mail: [Jurgita.Zekonyte@port.ac.uk](mailto:Jurgita.Zekonyte@port.ac.uk)

21

22

23 **Abstract**

24           Accumulation of amyloid- $\beta$  ( $A\beta$ ) in plaques in the brain and in artery walls as  
25 cerebral amyloid angiopathy indicates a failure of elimination of  $A\beta$  from the brain with age  
26 and Alzheimer's disease. A major pathway for elimination of  $A\beta$  and other soluble  
27 metabolites from the brain is along basement membranes within the walls of cerebral arteries  
28 that represent the lymphatic drainage pathways for the brain. The motive force for the  
29 elimination of  $A\beta$  along this perivascular pathway appears to be the contrary (reflection)  
30 wave that follows the arterial pulse wave. Following injection into brain parenchyma,  $A\beta$   
31 rapidly drains out of the brain along basement membranes in the walls of cerebral arteries;  
32 such drainage is impaired in apolipoprotein E  $\epsilon$ 4 (ApoE4) mice. For drainage of  $A\beta$  to occur  
33 in a direction contrary to the pulse wave some form of attachment to basement membrane  
34 would be required to prevent reflux of  $A\beta$  back into the brain during the passage of the  
35 subsequent pulse wave. In this study, we show first that apolipoprotein E co-localizes with  
36  $A\beta$  in basement membrane drainage pathways in the walls of arteries. Secondly, we show by  
37 Atomic Force Microscopy that attachment of ApoE4/ $A\beta$  complexes to basement membrane  
38 laminin is significantly weaker than ApoE3/ $A\beta$  complexes. These results suggest that  
39 perivascular elimination of ApoE4/ $A\beta$  complexes would be less efficient than with other  
40 isoforms of apolipoprotein E, thus endowing a higher risk for Alzheimer's disease.  
41 Therapeutic correction for ApoE4/ $A\beta$ /laminin interactions may increase the efficiency of  
42 elimination of  $A\beta$  in the prevention of Alzheimer's disease.

43

44 **Keywords:** Apolipoprotein E, perivascular clearance pathways, laminin, atomic force  
45 microscopy, amyloid- $\beta$ . Cerebral amyloid angiopathy, Alzheimer's disease

46

## 47 **1. Introduction**

48 A key feature of Alzheimer's disease pathology is the extracellular accumulation of  
49 soluble amyloid- $\beta$  ( $A\beta$ ) and of insoluble  $A\beta$  as plaques in brain parenchyma and in the walls  
50 of cerebral arteries as cerebral amyloid angiopathy (CAA) [1, 2]. These features indicate that  
51 there is a failure of elimination of  $A\beta$  from the brain with increasing age and in Alzheimer's  
52 disease [3]. Mechanisms for elimination of  $A\beta$  from the brain include enzymatic degradation  
53 by neprilysin within brain tissue and artery walls; absorption of  $A\beta$  into the blood mediated  
54 by low density lipoprotein receptor-1 and elimination by lymphatic drainage along basement  
55 membranes in the walls of cerebral capillaries and arteries [4]. Accumulation of insoluble  
56 fibrillar  $A\beta$  in the walls of capillaries and arteries in CAA reflects failure of elimination of  
57  $A\beta$  along lymphatic drainage pathways with age and Alzheimer's disease [5].

58 When soluble tracers, including  $A\beta$ , are injected into the brain parenchyma, they are  
59 rapidly eliminated along basement membranes of capillaries towards cervical lymph nodes  
60 [6, 7]. The pattern of deposition of  $A\beta$  in the walls of capillaries and arteries in human CAA  
61 exactly mirrors the lymphatic drainage pathways defined in experimental tracer studies [5].  
62 Tracers and  $A\beta$  appear to leave the walls of the carotid artery in the neck at the level of  
63 cervical lymph nodes as they drain from the brain to regional lymph nodes in the neck [6, 8].  
64 Perivascular drainage of  $A\beta$  from the brain is impaired with age as shown experimentally and  
65 by the presence of CAA in aging humans [9].  $A\beta$  secreted by amyloid precursor protein  
66 (APP)-transgenic mice harboring the Swedish double mutation driven by a neuron specific  
67 promoter is observed in the perivascular drainage pathways as CAA co-localized with  
68 apolipoprotein E (ApoE) [1]. Furthermore, perivascular drainage of  $A\beta$  is impaired in mice  
69 expressing human apolipoprotein E  $\epsilon$ 4 (ApoE4) suggesting that the risk factor for  
70 Alzheimer's disease in patients possessing the  $\epsilon$ 4 allele of ApoE may be related to a failure of  
71 elimination of  $A\beta$  from brain [10].

72           Studies on the motive force for perivascular drainage of A $\beta$  from the brain suggest  
73 that solutes are driven along basement membranes in the walls of arteries by the contrary  
74 (reflection) wave that follows the pulse wave [11]. In order for this mechanism to function  
75 effectively, some form of attachment of transported material to basement membrane proteins  
76 would be required in order to prevent reflux of material during passage of the pulse wave  
77 itself. If no attachment activity were present, A $\beta$  and other solutes would oscillate within the  
78 basement membrane rather than be driven rapidly out of the brain as has been observed  
79 experimentally. One of the major candidates for performing such attachment activity for A $\beta$   
80 is ApoE.

81           ApoE is the predominant lipoprotein in the brain and regulates transport of cholesterol  
82 from astrocytes to neurons [12-14]. Three *APOE* alleles ( $\epsilon$ 2,  $\epsilon$ 3 and  $\epsilon$ 4) encode the production  
83 of corresponding protein isoforms (E2, E3 and E4). Binding of A $\beta$  to ApoE has been  
84 proposed as a mechanism by which A $\beta$  is transported across the blood-brain barrier [4] and  
85 levels of ApoE are lower in ApoE4-positive individuals than in ApoE3 carriers [15]. Recent  
86 work has demonstrated minimal direct physical interaction between ApoE and soluble A $\beta$   
87 within the cerebrospinal fluid [16]. Thus, the role of ApoE in mediating the clearance of A $\beta$   
88 from the brain remains unresolved.

89           Since A $\beta$ 40 is the predominant type of A $\beta$  found in CAA [17], in the present study we  
90 tested the hypothesis that interactions of A $\beta$ 40 with protein components of cerebral vascular  
91 basement membranes, such as laminin, are stronger in the presence of ApoE3 than in the  
92 presence of apoE4. If this hypothesis is substantiated, it would suggest that perivascular  
93 drainage of A $\beta$  in individuals possessing ApoE4 would be less efficient due to defective  
94 attachment of A $\beta$ /ApoE4 complexes to basement membranes during perivascular lymphatic  
95 drainage. This would ultimately lead to failure of elimination of A $\beta$  from the brain and its  
96 deposition in artery walls as CAA. .

97 In order to test the hypothesis, we first identified the location of ApoE in relation to  
98 fibrillary A $\beta$  within basement membranes in the walls of arteries in AD. Secondly, we  
99 performed single-molecule force spectroscopy with an atomic force microscope (AFM) in  
100 order to determine the force of attachment between A $\beta$ /ApoE4 complexes and the basement  
101 membrane protein, laminin. We then compared the attachment forces of A $\beta$ /ApoE4  
102 complexes with those of A $\beta$ /ApoE3.

103

## 104 **2. Materials and Methods**

### 105 **2.1 Materials for AFM tip functionalization**

106 Analytical grade materials used for AFM tip functionalization were obtained from  
107 Sigma Aldrich, UK. The following chemicals were used: ethanol, chloroform, ethanolamine  
108 hydrochloride (ethanolamine-HCl), dimethylsulfoxide (DMSO), triethylamine (TEA),  
109 sodium hydroxide (NaOH), sodium cyanoborohydride (NaCNBH<sub>3</sub>). Aldehyde-PEG-NHS  
110 linker was purchased from Institute of Biophysics, University of Linz, Austria. Human  
111 recombinant laminin-511 was purchased from (BioLamina, Sweden), while human A $\beta$ 40  
112 (referred to as A $\beta$  for the rest of the manuscript), human ApoE3 and human ApoE4 were  
113 from Cambridge Bioscience (Cambridge, UK).

114

### 115 **2.2 Immunofluorescence of human tissue**

116 Paraffin sections from 5 cases diagnosed with Alzheimer's disease from the South  
117 West Dementia Brain Bank, Frenchay Hospital, Bristol were utilised for immunostaining.  
118 Sections of middle frontal gyrus were immunostained with antibodies specific for A $\beta$ 42  
119 (clone 21F12, 1:4000), pan-apolipoprotein E (pan-apoE, clone 5F6, 1:2000) provided by Elan  
120 Pharmaceuticals Inc. (USA). We could not access an antibody specific for A $\beta$ 40 that worked  
121 on human tissue, so we used A $\beta$ 42, as we know that A $\beta$ 42 becomes entrapped in the

122 cerebrovascular amyloid deposits [18, 19]. Smooth muscle actin (SMA: clone 1A4, Dako,  
123 UK, 1:100) was used to identify smooth muscle cells in the blood vessel walls.

124 Immunostaining was performed using the appropriate antigen retrieval methods for  
125 each primary antibody. For A $\beta$ 42, pan-apoE and ApoE E4 sections were pre-treated with  
126 neat formic acid. Triple immunostaining was detected using AF594 (red, A $\beta$ 42) or AF633  
127 (blue, pan-apoE) fluorochromes conjugated with biotinylated secondary antibodies (Life  
128 Technologies, UK) and SMA-FITC (Abcam, UK, 1:200, green), respectively. A Leica SP5  
129 confocal scanning microscope was used for imaging.

130

## 131 **2.3 Atomic force microscope measurements**

### 132 **2.3.1 Functionalization of AFM measuring tips**

133 The AFM silicon nitride tips (MSNL-10, Bruker, UK) were functionalized with the  
134 desired protein following three modification steps: (1) amino functionalization, (2)  
135 modification with aldehyde-PEG-NHS linker, and (3) ligand coupling. AFM cantilevers were  
136 washed in chloroform three times and dried under a stream of nitrogen before tips were  
137 subjected to modification. Amino functionalization was done by esterification with  
138 ethanolamine at room temperature [20]. AFM tips were then placed in a closed container with  
139 the ethanolamine-HCl solution, left overnight, washed three times in DMSO and ethanol and  
140 dried under a stream of nitrogen. Subsequent functionalization steps were performed  
141 following a custom tip modification protocol provided by Agilent Technologies, Inc. [21].  
142 The PEG linker was immobilized on aminated AFM probes by the NHS ester terminus (step  
143 2). 3.3 mg of aldehyde-PEG-NHS linker was dissolved in 1 ml chloroform, and transferred  
144 into a small glass reaction chamber. 10  $\mu$ l of triethylamine was added before amino-  
145 functionalized AFM tips were immersed into the solution. The chamber was covered to  
146 prevent chloroform evaporation. After 1.5 hours, tips were removed from the solution,

147 washed three times in chloroform, and dried under the stream of nitrogen. The use of PEG  
148 spacer, as an intermittent link for biomolecule attachment to the cantilever, provides  
149 important advantages in molecular recognition force spectroscopy [22-26]. The linker is  
150 chemically and physically inert, allowing rapid and free reorientation of biomolecules. The  
151 spacing between molecule and the tip reduces the likelihood of molecules being crushed  
152 during the probe-surface contact. Non-linear elastic properties of PEG make it easy to  
153 discriminate between the non-specific and specific interaction events.

154 Proteins (Laminin, ApoE3, or ApoE4) were immobilized on AFM probes using the  
155 amine-amine reactive linker aldehyde-PEG-NHS. A sheet of parafilm was pressed into a  
156 glass petri dish. AFM cantilever chips were set onto the film in a circular “wagon wheel”  
157 pattern so that the tips were pointed upward and inward. 10 - 30  $\mu$ l of the protein solution was  
158 applied onto the cantilevers. The proteins were allowed to react for one hour to couple via  
159 intrinsic amino groups to the aldehyde-function of the PEG linker on the tip. After one hour,  
160 5  $\mu$ l of 1M ethanolamine was added to the protein solution drop to inactivate unreacted  
161 aldehyde groups.

162

### 163 **2.3.2 Substrate preparation for AFM experiments**

164 Substrates for AFM experiments were prepared as follows: 20  $\mu$ l of protein solution,  
165 i.e. A $\beta$ , ApoE3, ApoE4, or complexes of ApoE3 + A $\beta$  (1:1 molar ratio), and ApoE4 + A $\beta$   
166 (1:1 molar ratio). Complexes were left to react at 4°C for 1 hour. Solutions were added onto  
167 a freshly cleaved mica (Agar Scientific, UK) substrate which was already inserted into a  
168 liquid cell. 100  $\mu$ l of dH<sub>2</sub>O were added to a cell. Proteins were left to adsorb to the substrate  
169 for 30 min. The mica substrate was washed with water to ensure that only adsorbed proteins  
170 remained on the substrate.



171 A $\beta$  has a tendency to form large aggregates with time [27]. To maintain the solubility  
172 state of A $\beta$ , fresh protein was deposited on the mica every 4 hours, and a new functionalized  
173 AFM tip was used in the experiments. Images of A $\beta$  were captured immediately after  
174 deposition and before the possible A $\beta$  rearrangement, i.e. after 4 hours. No A $\beta$  agglomeration  
175 in fibrillar form was observed on the mica during any stage of the experiment.

176

### 177 **2.3.3 Single molecule force spectroscopy experiments**

178 Sample imaging and molecular force spectroscopy experiments were performed in  
179 water using Agilent 5500 Scanning Probe Microscopy, MAC III, Agilent Technologies, US.  
180 Images were acquired using the same cantilevers in contact mode. Actual constant values of  
181 AFM cantilevers were measured in liquid using a built-in thermal noise method [28] before  
182 each experimental set. Determined force constant was used to calculate actual loading and  
183 unbinding forces. Force spectroscopy data were acquired at loading rates ranging from 3000  
184 – 160000 pN/s, corresponding to retraction rates of 0.08 – 3  $\mu$ m/s. At least 1000 curves were  
185 recorded for each experimental condition. The following tip-substrate pairs were measured:  
186 Laminin - A $\beta$ , Laminin - ApoE3, Laminin - ApoE4, or Laminin (on the tip), against  
187 complexes of ApoE3 + A $\beta$ , or ApoE4 + A $\beta$ . In a separate run of experiments, we used  
188 ApoE3 on the tip and A $\beta$  as a substrate, or ApoE4 on the tip and A $\beta$  as a substrate. All  
189 experiments were repeated independently three times, allowing 2 – 3 weeks between each  
190 repeat.

191

192

193

194

### 195 2.3.4 Data Analysis

196 PicoView 1.10 and PicoImage (Agilent Technologies, US) software were used for  
197 data acquisition and image analysis, respectively. Force curves were analysed using PUNIAS  
198 macro software (<http://punias.voila.net/>). From several hundred single molecule unbinding  
199 events, the probability density function (PDF) was constructed as described in [29, 30]. The  
200 PDFs were fitted with the equation:

$$201 \quad p(F) = \sum_{i=1}^N \frac{1}{N\sigma_i\sqrt{2\pi}} \exp\left(-\frac{(F-\mu_i)^2}{2\sigma_i^2}\right) \quad (1)$$

202 where  $p(F)$  is the estimate for the PDF that the bond will break at force  $F$ ,  $\mu_i$  and  $\sigma_i$  are  
203 rupture force and accuracy respectively, with the sum running over all  $N$  (several hundred in  
204 our case) rupture events. PDF gives the statistical distribution of rupture forces (termed as  
205 “unbinding force”). The most probable unbinding force was then determined by fitting Gauss  
206 function to the estimated PDF using Origin analytical software.

207 In a single barrier model [31], the unbinding force  $F_U$  is given as a function of the loading  
208 rate:

$$209 \quad F_U = \frac{k_B T}{x_\beta} \ln(r) - \frac{k_B T}{x_\beta} \ln\left(k_{off} \frac{k_B T}{x_\beta}\right) \quad (2)$$

210 where  $k_B T$  is the thermal energy (4.1 pNnm at room temperature),  $k_{off}$  (1/s) is the dissociation  
211 rate constant,  $x_\beta$  is a length scale in nm describing the separation of the receptor-ligand pair  
212 between the bound and the transition state,  $r$  (pN/s) is the loading rate. The parameters  $x_\beta$  and  
213  $k_{off}$  were determined by fitting  $F_U$  against  $\ln(r)$ .

214

215

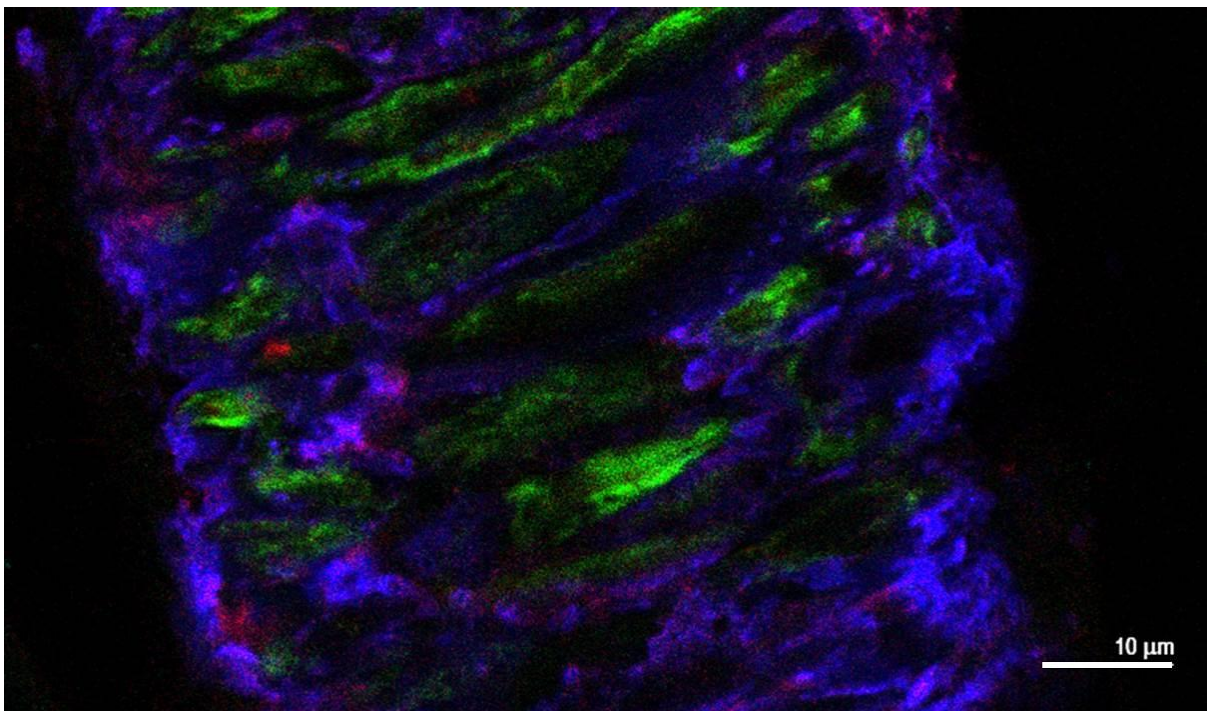
216

217 **3. Results**

218 **3.1 Immunofluorescence**

219 A $\beta$ 42 was observed in the walls of blood vessels from brains with Alzheimer's  
220 disease (Figure 1). ApoE was also observed in the walls of arteries, between the layers of  
221 smooth muscle cells and co-localized with A $\beta$ 42 (Figure 1).

222



223 **Figure 1.** Triple immunostaining for Amyloid- $\beta$  (A $\beta$ ) 1-42 (red), pan-Apolipoprotein E  
224 (ApoE) (blue), smooth muscle actin (green) of a leptomenigeal artery of a case of  
225 Alzheimer's disease. A $\beta$ 42 co-localizes with apolipoprotein E (magenta) adjacent to smooth  
226 muscle actin, suggesting that A $\beta$  and ApoE co-localize in the basement membranes of the  
227 smooth muscle tunica media. Confocal Leica SP5 image, a 63 objective was used, scale bar  
228 10  $\mu$ m.

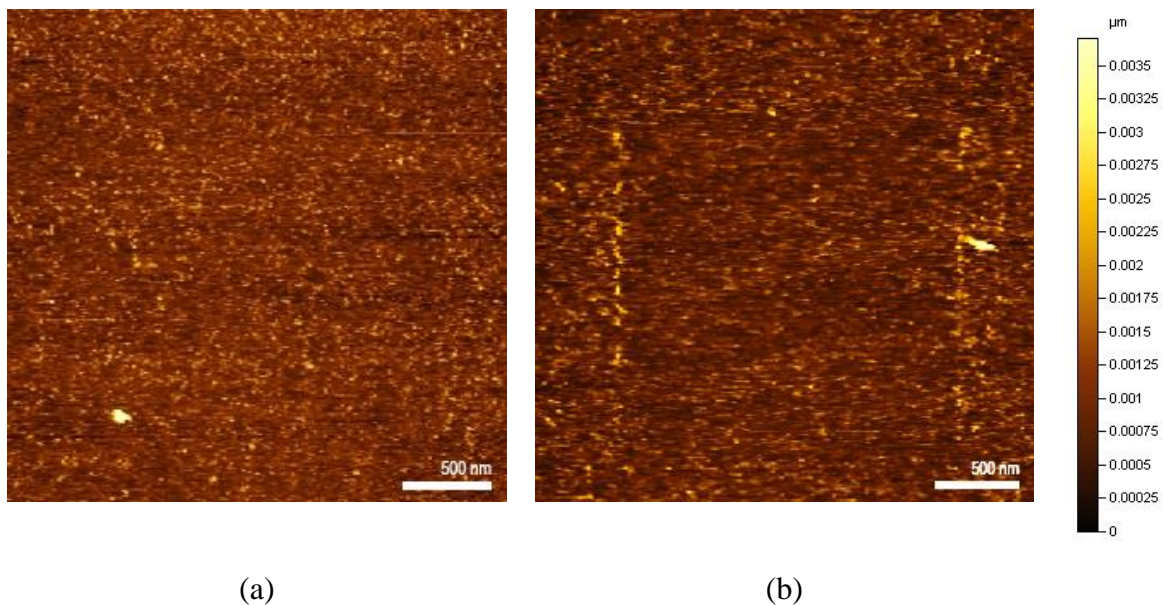
229

230

231 **3.2 Molecule force spectroscopy**

232 Force-spectroscopy experiments were performed to study the reciprocal influence of  
233 different isoforms of ApoE and A $\beta$  on their binding interactions with laminin. The protein  
234 adsorption on the mica, its conformation and size was investigated by contact-mode AFM  
235 imaging in liquid. As an example, Figure 2a shows A $\beta$  assemblies on the substrate.  
236 Scratching away adhered molecules with higher force, gave 2 x 2  $\mu$ m area of bare (or almost  
237 bare) mica (Figure 2b). This simple experiment further confirmed protein presence on the  
238 surface. Furthermore, it also indicates that A $\beta$  is in the form of small oligomers (molecules  
239 were of about  $5 \pm 0.5$  nm in height) instead of fibrils as described in Refs. [32, 33] or large  
240 agglomerates. ApoEs were measured to be  $15 \pm 2$  nm in height, and complexes of A $\beta$  with  
241 ApoE3/4 were  $20 \pm 2$  nm.

242



243 **Figure 2.** Contact-mode AFM images in liquid of A $\beta$  deposited on mica (a). The presence of  
244 protein molecules was proved by scratching the proteins with higher force in an area of 2 x 2  
245  $\mu$ m (b). Scale bar – 500 nm.

246

247 To study specific binding of tip-bound protein to mica-bound protein by force  
248 spectroscopy, the functionalized tip was repeatedly brought into contact with the protein and  
249 retracted at constant load and velocity. Figure 3a shows an example of typical force-distance  
250 curve with a single recognition event. The cycle starts at a point 1 which corresponds to the  
251 free cantilever, when the tip is far away from the substrate. The probe comes in contact with  
252 the surface at point 2, and bends further until it reaches point 3. During unloading, the  
253 cantilever relaxes to reach point 4, which usually corresponds to the point of contact. If there  
254 is specific interaction between biomolecules, the unloading curve follows the pass through  
255 steps 5-7. The cantilever begins to deflect in a non-linear fashion. This characteristic  
256 signature peak results from the stretching of the polymer linker, and identifies specific ligand-  
257 receptor binding. The force increases until enough energy is transferred to break the bond  
258 (points 6 to 7), where  $F_U$  indicates an unbinding force in pN. The tip and substrate are  
259 completely separated at this point. To ensure that the measured unbinding event is specific to  
260 the ligand-receptor interaction, the force-displacement curves between the functionalized tip  
261 and clean mica in an aqueous environment were recorded. As expected, all loading and  
262 unloading curves were identical in control experiments, Figure 3b.

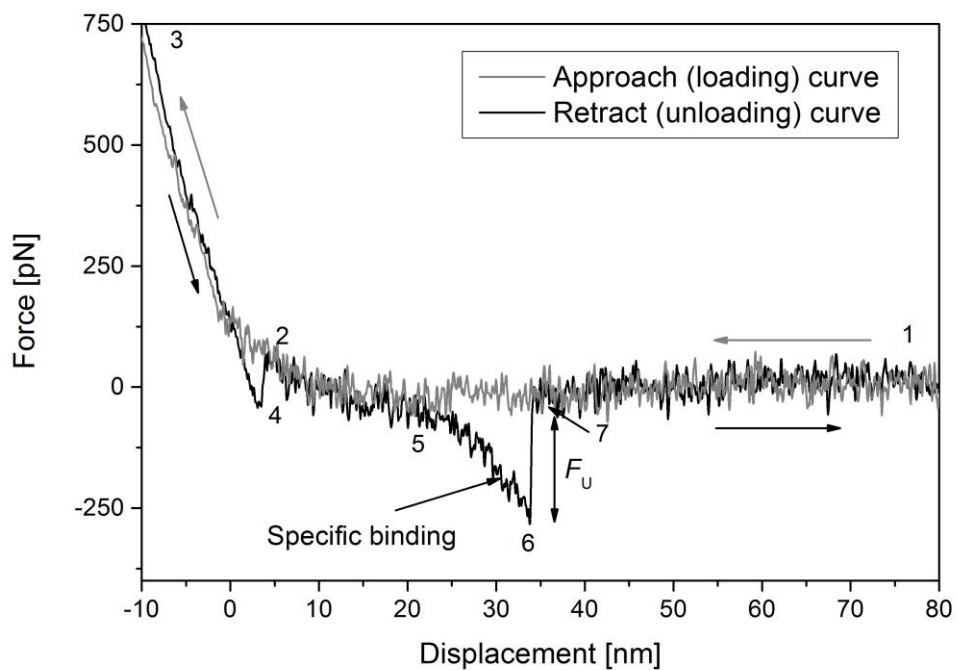
263

264

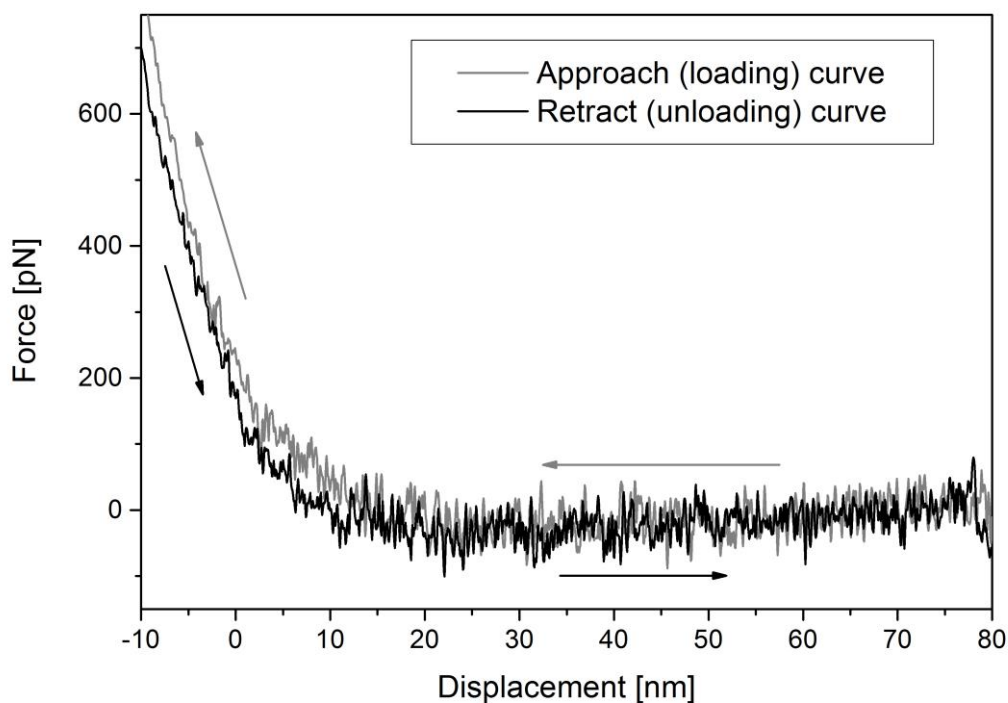
265

266

267



(a)

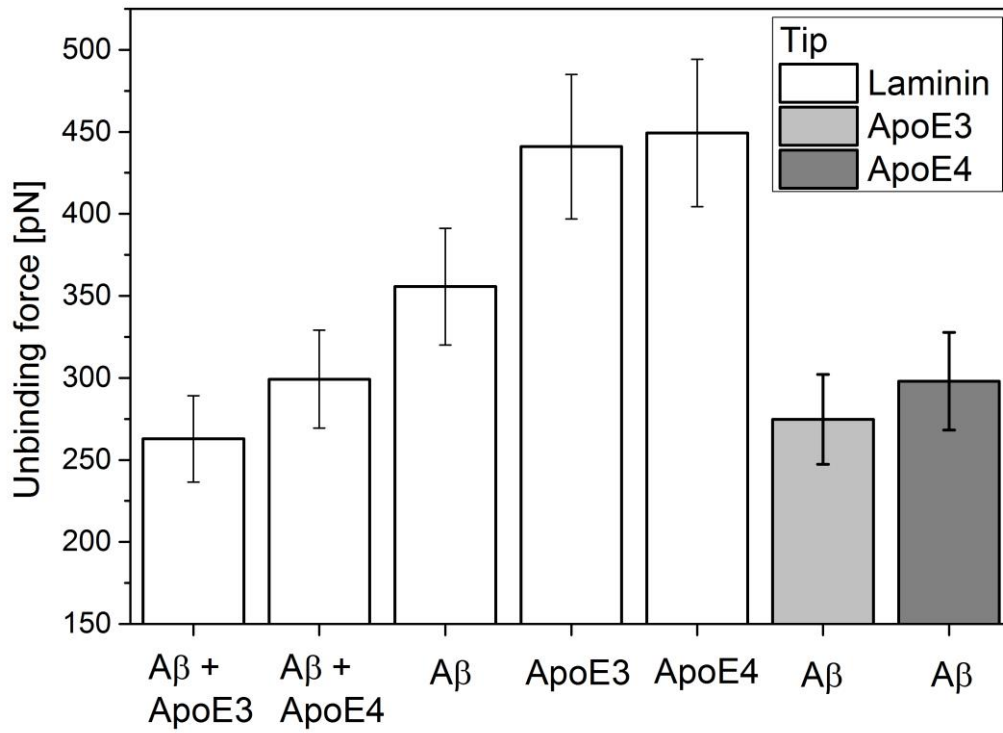


(b)

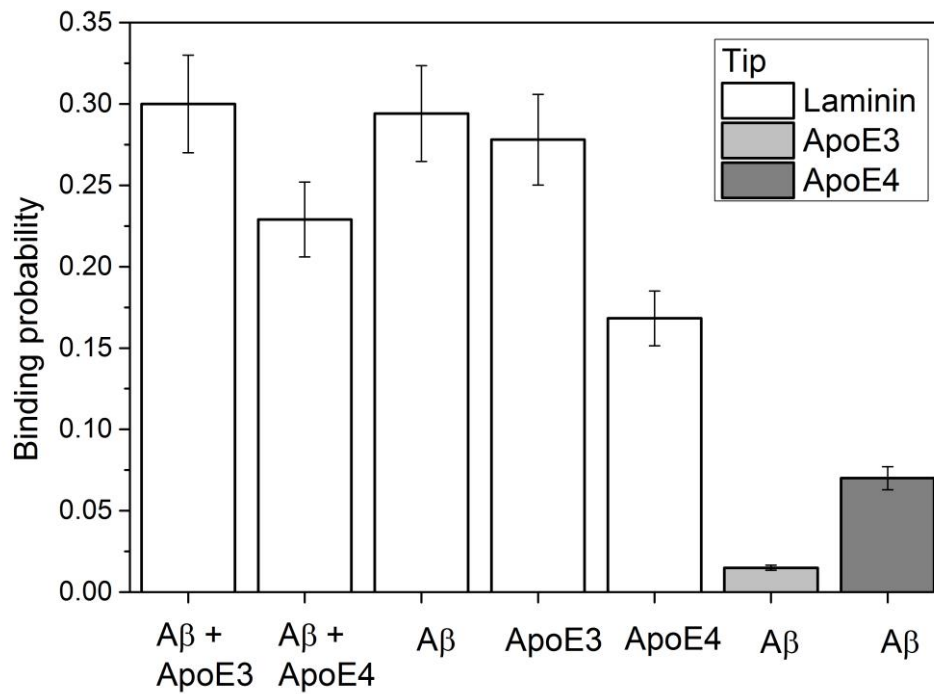
268 **Figure 3.** Example of force-displacement curves obtained during single molecule force  
 269 spectroscopy experiments for an experimental set tip - ApoE3, substrate - A $\beta$ . (a) Typical  
 270 force-displacement cycle with a single specific interaction. See text for explanation. (b)  
 271 Control - no interaction between biomolecules attached to the tip and clean mica substrate.

272 Force-displacement cycles were analysed as described in materials and methods. The  
273 most probable unbinding force and binding probabilities (BP) were calculated using  
274 Equations 1 and 2. The  $F_U$  and binding probability results for various ligand-receptor pairs  
275 recorded at 1 Hz with 100-300 nm amplitude, resulting in loading rates from 15,000 – 70,000  
276 pN/s, are presented in Figure 4. The unbinding forces between laminin and ApoE3 and  
277 between laminin and apoE4 are the same ( $450 \pm 50$  pN), Figure 4a. However, when A $\beta$  was  
278 added to ApoE, less energy was required to detach a laminin molecule from any of the  
279 complexes ( $\sim 270 \pm 25$  pN). It was also noted that unbinding of ApoE3 and ApoE4 from A $\beta$   
280 occurred with similar force of  $\sim 270 \pm 25$  pN, while laminin bonded to A $\beta$  at forces of  $350 \pm$   
281  $35$  pN.

282 The binding probability was defined as the probability of recording an unbinding  
283 event in a force-distance cycle in relation to all recorded cycles, i.e. how many curves with  
284 specific recognition were recorded out of 1000 measured cycles. Results of binding  
285 probability for various tip-substrate interaction are given in Figure 4b, where BP of 1 would  
286 correspond to 100%, 0.3 = 30%, and so on. Laminin tended to bind more frequently to  
287 ApoE3, A $\beta$ , and A $\beta$ +ApoE3 complex with a probability of  $\sim 30 \pm 3\%$ . BP of laminin to  
288 ApoE4 was calculated to be  $15 \pm 1.5 \%$ , and for A $\beta$ +ApoE4 complex it was  $22 \pm 2 \%$ . Very  
289 few binding events were recorded between ApoE3/4 (tip) and A $\beta$  (substrate), where 7% of all  
290 specific recognition curves were recorded for ApoE4 - A $\beta$  interaction, and 2% for ApoE4 -  
291 A $\beta$  (Figure 4b, grey columns). A $\beta$  was always immobilized on the mica, and so the protein  
292 orientation might have been such that binding sites were directed towards the substrate  
293 leaving very few sites exposed. In this case, ApoEs attached to the AFM tip would hardly  
294 bind to A $\beta$ . If this were the case, similar results should be observed between laminin (tip) and  
295 A $\beta$  (substrate). But experimental binding probability between laminin and A $\beta$  was 30%, and  
296 so this would indicate that ApoEs do not interact with A $\beta$  so avidly.



(a)



(b)

297 **Figure 4.** (a) Most probable unbinding force,  $F_U$ , and (b) specific binding probability for  
 298 various tip-substrate pairs. Results are given for force-displacement cycles obtained at 1 Hz  
 299 with 100 – 300 nm amplitude.



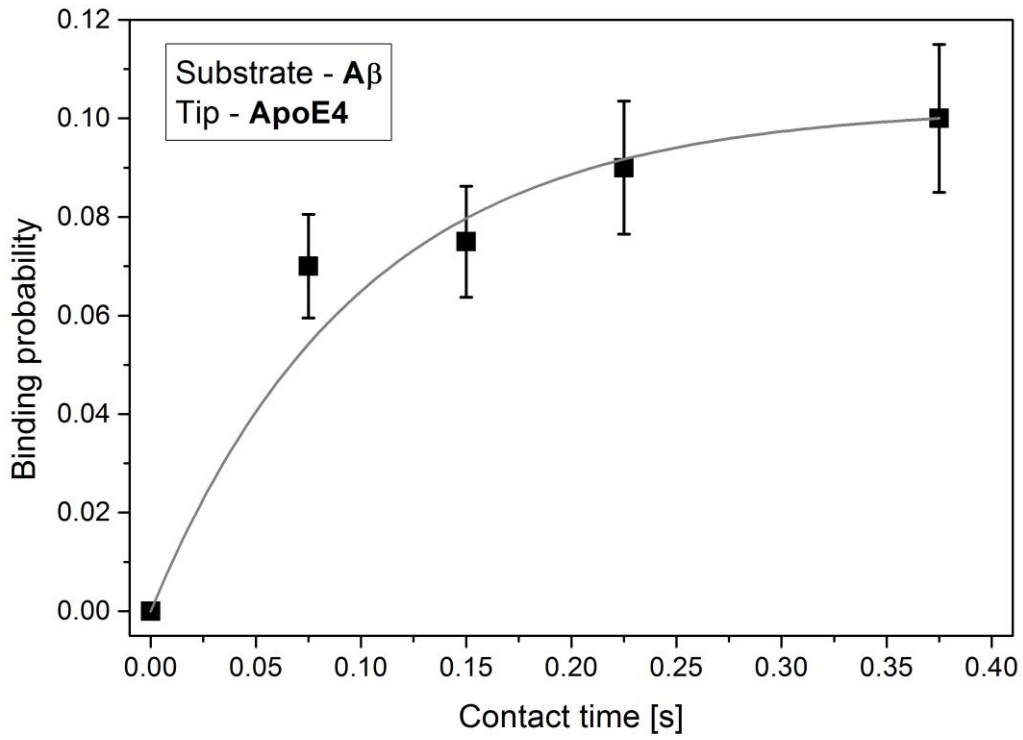
### 300 3.3 Kinetic constants and affinities

301 The parameters of prime interest in describing any biological ligand-receptor system  
302 are the rates of spontaneous association (or on-rate,  $k_{on}$ ), dissociation (off-rate,  $k_{off}$ ), and their  
303 ratio the dissociation constant (also known as affinity)  $K_D = k_{off}/k_{on}$  which describes the  
304 equilibrium behaviour. To calculate association and dissociation constants, molecular force  
305 spectroscopy experiments were carried out in a range of loading rates from 3000 – 160000  
306 pN/s, and tip-substrate contact times 0.001 – 0.5 s. To estimate kinetic on-rate constant,  $k_{on}$ ,  
307 from single molecule unbinding force measurements, it is necessary to determine interaction  
308 time  $\tau$  (the time required for half maximal recognition probability) and effective  
309 concentration  $c_{eff}$ , for  $k_{on} = (\tau c_{eff})^{-1}$ [23, 34, 35]. The effective concentration is described as a  
310 number of binding receptor molecules within the effective volume accessible for free  
311 equilibrium interaction, and is explained in detail elsewhere [23, 34, 35]. The interaction time  
312 was calculated from the binding probability at different encounter times by fitting  $P = A(1 -$   
313  $\exp(- (t - t_0)/\tau))$  (where  $t_0$  is a lag time,  $A$  is the maximum observable binding probability)  
314 [34]. An example is shown in figure Figure 5(a) for ApoE4 interaction with A $\beta$ .

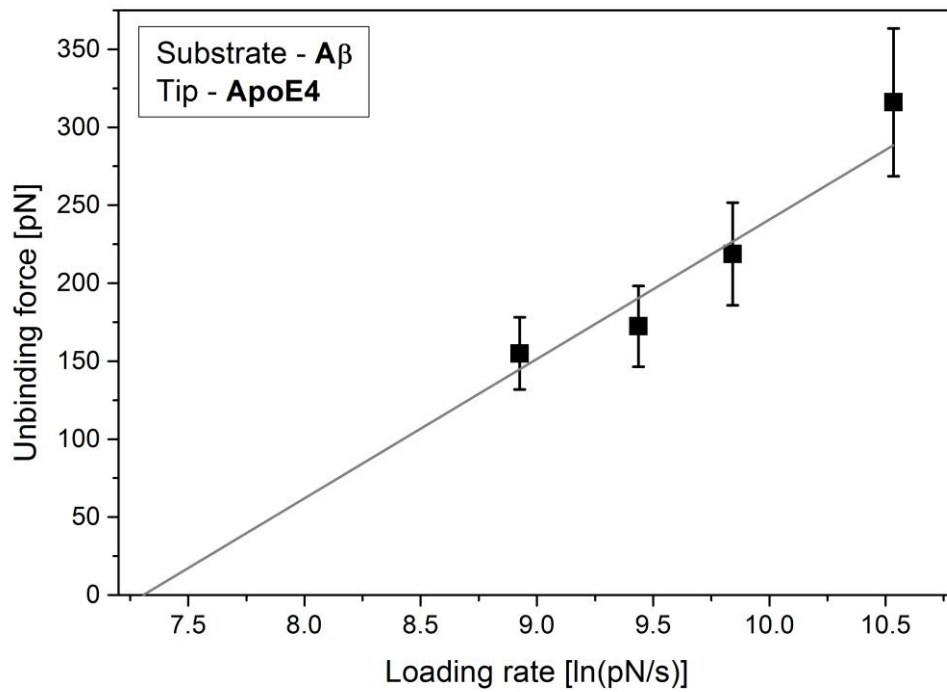
315 Furthermore, according to single barrier theory, the unbinding force rises linearly with  
316 respect to logarithmically increasing loading rate [30, 36, 37]. A linear increase of the most  
317 probable unbinding force versus loading rate was observed for all measured interactions. As  
318 an example, Figure 5(b) demonstrates unbinding force dependence on loading rate for ApoE4  
319 interaction with A $\beta$ . The off-rate is determined from the linear fit extrapolated at zero force  
320 [36, 37]. The slope of the fit corresponds to  $k_{\beta}T/x_{\beta}$  in Equation 2. The intercept at zero force

321 allows the calculation of  $k_{off}$  from Equation 2,  $\left(-\frac{k_{\beta}T}{x_{\beta}} \ln\left(k_{off} \frac{k_{\beta}T}{x_{\beta}}\right)\right)$ .

322



(a)



(b)

323 **Figure 5.** Kinetics of ligand-receptor binding. (a) Binding probability as a function of contact  
 324 time. Solid line is the result of least- squares fit. (b) Unbinding force as a function of loading  
 325 rate.

326

327 Calculated rate constants and affinities for all AFM measured ligand-receptor pairs is  
328 given in Table 1. The results for all AFM measurements demonstrate that A $\beta$  + ApoE3  
329 complex has a stronger binding to laminin than A $\beta$  + ApoE4.

330

331 **Table 1.** Association ( $k_{on}$ ) and dissociation ( $k_{off}$ ) rates, and affinity ( $K_D$ ) obtained by AFM.  
332 The lower  $K_D$  value indicates stronger interaction. A $\beta$  + ApoE3 has a stronger binding to  
333 laminin, compared to A $\beta$  + ApoE4.

Tip	Substrate	$k_{on}$ (1/Ms)	$k_{off}$ (1/s)	$K_D$ (1/M)
ApoE3	A $\beta$	$2.26 \times 10^4$	0.01091	$4.83 \times 10^{-7}$
ApoE4	A $\beta$	$1.08 \times 10^5$	0.01025	$9.45 \times 10^{-8}$
Laminin	A $\beta$	$1.10 \times 10^6$	0.01241	$1.13 \times 10^{-8}$
	ApoE3	$2.08 \times 10^6$	0.00541	$2.60 \times 10^{-9}$
	ApoE4	$1.07 \times 10^6$	0.00527	$4.94 \times 10^{-9}$
	A $\beta$ + ApoE3	$1.23 \times 10^6$	0.018	$1.46 \times 10^{-8}$
	A $\beta$ + ApoE4	$1.46 \times 10^5$	0.02224	$1.52 \times 10^{-7}$

334

335

#### 336 4. Discussion

337 The results of the present study have shown that ApoE and A $\beta$ 42 co-localize within  
338 basement membranes of the cerebral vasculature that form the elimination pathways for A $\beta$   
339 from the brain, consistent with A $\beta$  being eliminated from the brain as a complex with ApoE  
340 [12]. Electron paramagnetic resonance spectroscopy study of the interactions between

341 apolipoprotein E and oligomers of A $\beta$ 40 demonstrate that ApoE3 has a higher affinity for  
342 A $\beta$ 40 compared to ApoE4 [38]. Our own data show stronger binding of A $\beta$ 40 to ApoE4  
343 compared with ApoE3. Other studies have shown that ApoE4 binds A $\beta$  with higher affinity  
344 compared with ApoE3 and this is reversed when using lipidated forms of ApoE [39, 40] .  
345 More recently, using HEK-293 cells expressing ApoE3 or ApoE4 and A $\beta$ 42 it was shown  
346 that the interactions between ApoE4 and A $\beta$ 42 are weaker compared with ApoE3- A $\beta$ 42,  
347 with ApoE3-A $\beta$  complexes saturable and dependent on A $\beta$  concentrations [41]. We did not  
348 use A $\beta$ 42 in this study, but A $\beta$ 40, the type predominantly found in the walls of blood vessels  
349 and we used a ratio of A $\beta$ -ApoE of 1:1, as our aim was to concentrate on the interaction of  
350 the A $\beta$ 40-ApoE3/4 complexes with the laminin component of the basement membranes.

351 We found that the complex A $\beta$  + ApoE4 interacted with laminin less avidly ( $K_D =$   
352  $1.52 \times 10^{-7} \text{ M}^{-1}$ ) compared to the complex A $\beta$  + ApoE3 ( $K_D = 1.46 \times 10^{-8} \text{ M}^{-1}$ ). These results,  
353 together with our mathematical modelling studies (4), suggest that the perivascular clearance  
354 of soluble A $\beta$  along cerebrovascular basement membranes may be slower in ApoE4 carriers,  
355 compared to ApoE3 carriers, due to a lack of biophysical interaction between A $\beta$  and  
356 individual components of basement membranes (in this case laminin). Less efficient  
357 biophysical interaction between A $\beta$  + ApoE4 and basement membrane proteins, such as  
358 laminin would mean that there would be weaker attachment to the basement membrane  
359 during passage of the pulse wave and ApoE4-A $\beta$  complexes may remain in the extracellular  
360 spaces as seeds for plaques, promoting inflammation [42, 43]. Thus A $\beta$  + ApoE4 would not  
361 be driven out of the brain along perivascular pathways as efficiently as A $\beta$  + ApoE3. This  
362 may be an important factor in the failure of elimination of A $\beta$  from the brain in ApoE4  
363 carriers and the consequent accumulation of A $\beta$  in the brain and artery walls and the  
364 development of Alzheimer's disease. Apolipoprotein E appears to be located in the

365 perivascular compartment of blood vessels in the human brain and co-localizes with A $\beta$  in  
366 Alzheimer's disease [44].

367 Elimination of A $\beta$  from the brain in Alzheimer's disease has been the major objective  
368 of a number of A $\beta$  immunotherapy trials. Although in many patients insoluble plaques of A $\beta$   
369 are cleared from cortical areas, an increase in the severity of CAA has been reported [45].  
370 This suggests that A $\beta$  cleared from the brain parenchyma becomes entrapped in the  
371 perivascular drainage pathways with the ultimate failure of elimination of A $\beta$  from the brain  
372 [45]. Recently it has also been demonstrated that A $\beta$  immunotherapy was associated with  
373 redistribution of ApoE from cortical plaques to cerebral vessel walls, mirroring the altered  
374 distribution of A $\beta$  42 from the plaques towards the walls of blood vessels [46], consistent  
375 with ApoE/A $\beta$  travelling as a complex. Complications are associated with A $\beta$   
376 immunotherapy, designated Amyloid Related Imaging Abnormalities (ARIA) [47]. Evidence  
377 suggests that ARIAs are due to vascular alterations, including increased severity of CAA. As  
378 ARIAs occur more frequently in AD patients who are *APOE*  $\epsilon$ 4 carriers than non- $\epsilon$ 4 carriers,  
379 the differential binding of A $\beta$ /apoE E3 and E4 to laminin demonstrated in this study may be  
380 relevant to the causation of ARIA as A $\beta$  is being removed from the brain.

381

## 382 **5. Conclusions**

383 The results of this study add to our knowledge of the dynamics of perivascular  
384 drainage and its importance for the elimination of A $\beta$  from the brain. Accumulation of  
385 soluble and insoluble A $\beta$  in brain parenchyma and in artery walls occurs with advancing age  
386 and is enhanced in those possessing the ApoE4 allele. Experimental and theoretical data  
387 indicate that vascular pulsations are the driving force for perivascular elimination of A $\beta$  with  
388 the contrary (reflection) wave driving A $\beta$  and other solutes out of the brain in the reverse

389 direction to blood flow [11]. Reduction in the amplitude of the pulse wave may occur as  
390 arteries stiffen with age and arteriosclerosis, thus reducing the motive force for the  
391 perivascular drainage of A $\beta$  and other solutes from the brain.

392 The present study suggests that the presence of ApoE4 further reduces the efficiency  
393 of perivascular elimination of A $\beta$  due to reduced attachment of ApoE4/A $\beta$  complexes to  
394 basement membranes in the drainage pathway, although the type of A $\beta$  and the lipidation  
395 status of ApoE are crucial [12]. Such reduced attachment may allow oscillation of A $\beta$  within  
396 the basement membrane during passage of the pulse wave and thus impair the progress of A $\beta$   
397 out of the brain along the perivascular pathways.

398 Therapeutic strategies that optimise attachment of soluble metabolites to basement  
399 membrane proteins may also optimise elimination of those metabolites from the brain. The  
400 present study has established a principle that could be developed in the future to test therapies  
401 for the prevention of Alzheimer's disease, based on manipulating the A $\beta$ -ApoE interactions  
402 with basement membrane proteins.

403

#### 404 **Acknowledgements**

405 We are grateful to Cheryl Hawkes for technical help, to the Engineering and Physical  
406 Sciences Research Council of UK and Alzheimer's Research UK for providing the funding  
407 for this study, to the South West Dementia Brain Bank for the brain tissue.

408

#### 409 **References**

- 410 [1] D.R. Thal, W.S.T. Griffin, R.A.I. de Vos, E. Ghebremedhin, Cerebral amyloid angiopathy  
411 and its relationship to Alzheimer's disease, *Acta Neuropathol*, 115 (2008) 599-609.
- 412 [2] D.R. Thal, A. Papassotiropoulos, T.C. Saido, W.S.T. Griffin, R.E. Mrak, H. Kolsch, K.  
413 Del Tredici, J. Attems, E. Ghebremedhin, Capillary cerebral amyloid angiopathy identifies a

- 414 distinct APOE epsilon 4-associated subtype of sporadic Alzheimer's disease, *Acta*  
415 *Neuropathol*, 120 (2010) 169-183.
- 416 [3] R.O. Carare, C.A. Hawkes, M. Jeffrey, R.N. Kalaria, R.O. Weller, Review: Cerebral  
417 amyloid angiopathy, prion angiopathy, CADASIL and the spectrum of protein elimination  
418 failure angiopathies (PEFA) in neurodegenerative disease with a focus on therapy, *Neuropath*  
419 *Appl Neuro*, 39 (2013) 593-611.
- 420 [4] R. Deane, A. Sagare, K. Hamm, M. Parisi, S. Lane, M.B. Finn, D.M. Holtzman, B.V.  
421 Zlokovic, apoE isoform-specific disruption of amyloid beta peptide clearance from mouse  
422 brain, *J Clin Invest*, 118 (2008) 4002-4013.
- 423 [5] R.O. Weller, M. Subash, S.D. Preston, I. Mazanti, R.O. Carare, Perivascular drainage of  
424 amyloid-beta peptides from the brain and its failure in cerebral amyloid angiopathy and  
425 Alzheimer's disease, *Brain Pathol*, 18 (2008) 253-266.
- 426 [6] I. Szentistvanyi, C.S. Patlak, R.A. Ellis, H.F. Cserr, Drainage of Interstitial Fluid from  
427 Different Regions of Rat-Brain, *Am J Physiol*, 246 (1984) F835-F844.
- 428 [7] R.O. Carare, M. Bernardes-Silva, T.A. Newman, A.M. Page, J.A.R. Nicoll, V.H. Perry,  
429 R.O. Weller, Solutes, but not cells, drain from the brain parenchyma along basement  
430 membranes of capillaries and arteries: significance for cerebral amyloid angiopathy and  
431 neuroimmunology, *Neuropath Appl Neuro*, 34 (2008) 131-144.
- 432 [8] Y. Shinkai, M. Yoshimura, Y. Ito, A. Odaka, N. Suzuki, K. Yanagisawa, Y. Ihara,  
433 Amyloid P-Proteins-1-40 and P-Proteins-1-42(43) in the Soluble Fraction of Extracranial and  
434 Intracranial Blood-Vessels, *Ann Neurol*, 38 (1995) 421-428.
- 435 [9] C.A. Hawkes, W. Hartig, J. Kacza, R. Schliebs, R.O. Weller, J.A. Nicoll, R.O. Carare,  
436 Perivascular drainage of solutes is impaired in the ageing mouse brain and in the presence of  
437 cerebral amyloid angiopathy, *Acta Neuropathol*, 121 (2011) 431-443.
- 438 [10] C.A. Hawkes, P.M. Sullivan, S. Hands, R.O. Weller, J.A.R. Nicoll, R.O. Carare,  
439 Disruption of Arterial Perivascular Drainage of Amyloid-beta from the Brains of Mice  
440 Expressing the Human APOE epsilon 4 Allele, *Plos One*, 7 (2012).
- 441 [11] D. Schley, R. Carare-Nnadi, C.P. Please, V.H. Perry, R.O. Weller, Mechanisms to  
442 explain the reverse perivascular transport of solutes out of the brain, *J Theor Biol*, 238 (2006)  
443 962-974.
- 444 [12] L.M. Tai, S. Mehra, V. Shete, S. Estus, G.W. Rebeck, G.J. Bu, M.J. LaDu, Soluble  
445 apoE/A beta complex: mechanism and therapeutic target for APOE4-induced AD risk, *Mol*  
446 *Neurodegener*, 9 (2014).
- 447 [13] S.R. Li, K. Oka, D. Galton, J. Stocks, Bst-1 Rflp at the Human Lipoprotein-Lipase (Lpl)  
448 Gene Locus, *Nucleic Acids Res*, 16 (1988) 11856-11856.
- 449 [14] S.R. Li, K. Oka, D. Galton, J. Stocks, Pvu-II Rflp at the Human Lipoprotein-Lipase (Lpl)  
450 Gene Locus, *Nucleic Acids Res*, 16 (1988) 2358-2358.
- 451 [15] D.R. Riddell, H. Zhou, K. Atchison, H.K. Warwick, P.J. Atkinson, J. Jefferson, L. Xu, S.  
452 Aschmies, Y. Kirksey, Y. Hu, E. Wagner, A. Parratt, J. Xu, Z.T. Li, M.M. Zaleska, J.S.  
453 Jacobsen, M.N. Pangalos, P.H. Reinhart, Impact of Apolipoprotein E (ApoE) Polymorphism  
454 on Brain ApoE Levels, *J Neurosci*, 28 (2008) 11445-11453.
- 455 [16] P.B. Verghese, J.M. Castellano, K. Garai, Y.N. Wang, H. Jiang, A. Shah, G.J. Bu, C.  
456 Frieden, D.M. Holtzman, ApoE influences amyloid-beta (A beta) clearance despite minimal

457 apoE/A beta association in physiological conditions, P Natl Acad Sci USA, 110 (2013)  
458 E1807-E1816.

459 [17] M.C. Herzig, W.E. Van Nostrand, M. Jucker, Mechanism of cerebral beta-amyloid  
460 angiopathy: Murine and cellular models, Brain Pathol, 16 (2006) 40-54.

461 [18] J. Nicoll, The effects of A beta immunization on the pathology of Alzheimer disease,  
462 Neurobiol Aging, 27 (2006) S15-S15.

463 [19] J.A.R. Nicoll, E. Barton, D. Boche, J.W. Neal, I. Ferrer, P. Thompson, C. Vlachouli, D.  
464 Wilkinson, A. Bayer, D. Games, P. Seubert, D. Schenk, C. Holmes, A beta species removal  
465 after A beta(42) immunization, J Neuropath Exp Neur, 65 (2006) 1040-1048.

466 [20] C.K. Riener, C.M. Stroh, A. Ebner, C. Klampfl, A.A. Gall, C. Romanin, Y.L.  
467 Lyubchenko, P. Hinterdorfer, H.J. Gruber, Simple test system for single molecule recognition  
468 force microscopy, Analytica Chimica Acta, 479 (2003) 59-75.

469 [21] Agilent Technologies □ PicoTREC Topography and Recognition Imaging System,  
470 User's Guide in, Agilent technologies, Inc., 2010.

471 [22] A. Ebner, P. Hinterdorfer, H.J. Gruber, Comparison of different aminofunctionalization  
472 strategies for attachment of single antibodies to AFM cantilevers, Ultramicroscopy, 107  
473 (2007) 922-927.

474 [23] P. Hinterdorfer, W. Baumgartner, H.J. Gruber, K. Schilcher, H. Schindler, Detection and  
475 localization of individual antibody-antigen recognition events by atomic force microscopy,  
476 Proceedings of the National Academy of Sciences of the United States of America, 93 (1996)  
477 3477-3481.

478 [24] V.J. Morris, Kirby, A.R., Gunning, A.P., Force spectroscopy, in: Atomic Force  
479 Microscopy for Biologist, Imperila College Press, 2010, pp. 356-396.

480 [25] G.S. Watson, Watson, J.A., Quantitative measurements of nano forces using Atomic  
481 Force Microscopy, VDM Verlag Dr. Muelller, 2008.

482 [26] W.F. Heinz, J.H. Hoh, Spatially resolved force spectroscopy of biological surfaces using  
483 the atomic force microscope, Trends in Biotechnology, 17 (1999) 143-150.

484 [27] D.R. Thal, M. Fandrich, Protein aggregation in Alzheimer's disease: A beta and tau and  
485 their potential roles in the pathogenesis of AD, Acta Neuropathol, 129 (2015) 163-165.

486 [28] J.L. Hutter, J. Bechhoefer, Calibration of Atomic-Force Microscope Tips, Review of  
487 Scientific Instruments, 64 (1993) 1868-1873.

488 [29] W. Baumgartner, P. Hinterdorfer, H. Schindler, Data analysis of interaction forces  
489 measured with the atomic force microscope, Ultramicroscopy, 82 (2000) 85-95.

490 [30] C. Rankl, F. Kienberger, H. Gruber, D. Blaas, P. Hinterdorfer, Accuracy estimation in  
491 force spectroscopy experiments, Japanese Journal of Applied Physics Part 1-Regular Papers  
492 Brief Communications & Review Papers, 46 (2007) 5536-5539.

493 [31] E. Evans, K. Ritchie, Dynamic strength of molecular adhesion bonds, Biophysical  
494 Journal, 72 (1997) 1541-1555.

495 [32] L.M. Jungbauer, C. Yu, K.J. Laxton, M.J. Ladu, Preparation of fluorescently-labeled  
496 amyloid-beta peptide assemblies: the effect of fluorophore conjugation on structure and  
497 function, J Mol Recognit, 22 (2009) 403-413.



498 [33] J.D. Harper, S.S. Wong, C.M. Lieber, P.T. Lansbury, Assembly of A beta amyloid  
499 protofibrils: An in vitro model for a possible early event in Alzheimer's disease,  
500 *Biochemistry*, 38 (1999) 8972-8980.

501 [34] C. Rankl, F. Kienberger, L. Wildling, J. Wruss, H.J. Gruber, D. Blaas, P. Hinterdorfer,  
502 Multiple receptors involved in human rhinovirus attachment to live cells, *Proceedings of the*  
503 *National Academy of Sciences of the United States of America*, 105 (2008) 17778-17783.

504 [35] W. Baumgartner, Gruber, H.J., Hinterdorfer, P., Drenckhahn, D., Affinity of trans-  
505 interacting VE-candherin determined by atomic force microscopy, *Single Molecules*, 1  
506 (2000) 119-122.

507 [36] F. Schwesinger, R. Ros, T. Strunz, D. Anselmetti, H.J. Guntherodt, A. Honegger, L.  
508 Jermutus, L. Tiefenauer, A. Pluckthun, Unbinding forces of single antibody-antigen  
509 complexes correlate with their thermal dissociation rates, *Proceedings of the National*  
510 *Academy of Sciences of the United States of America*, 97 (2000) 9972-9977.

511 [37] T. Strunz, K. Oroszlan, R. Schafer, H.J. Guntherodt, Dynamic force spectroscopy of  
512 single DNA molecules, *Proceedings of the National Academy of Sciences of the United*  
513 *States of America*, 96 (1999) 11277-11282.

514 [38] J. Petrlova, H.S. Hong, D.A. Bricarello, G. Harishchandra, G.A. Lorigan, L.W. Jin, J.C.  
515 Voss, A differential association of Apolipoprotein E isoforms with the amyloid-beta oligomer  
516 in solution, *Proteins*, 79 (2011) 402-416.

517 [39] M.J. Ladu, M.T. Falduto, A.M. Manelli, C.A. Reardon, G.S. Getz, D.E. Frail, Isoform-  
518 Specific Binding of Apolipoprotein-E to Beta-Amyloid, *J Biol Chem*, 269 (1994) 23403-  
519 23406.

520 [40] M.J. Ladu, T.M. Pederson, D.E. Frail, C.A. Reardon, G.S. Getz, M.T. Falduto,  
521 Purification of Apolipoprotein-E Attenuates Isoform-Specific Binding to Beta-Amyloid, *J*  
522 *Biol Chem*, 270 (1995) 9039-9042.

523 [41] L.M. Tai, T. Bilousova, L. Jungbauer, S.K. Roeske, K.L. Youmans, C.J. Yu, W.W.  
524 Poon, L.B. Cornwell, C.A. Miller, H.V. Vinters, L.J. Van Eldik, D.W. Fardo, S. Estus, G.J.  
525 Bu, K.H. Gylys, M.J. LaDu, Levels of Soluble Apolipoprotein E/Amyloid-beta (A beta)  
526 Complex Are Reduced and Oligomeric A beta Increased with APOE4 and Alzheimer Disease  
527 in a Transgenic Mouse Model and Human Samples, *J Biol Chem*, 288 (2013) 5914-5926.

528 [42] G.A. Rodriguez, L.M. Tai, M.J. LaDu, G.W. Rebeck, Human APOE4 increases  
529 microglia reactivity at A beta plaques in a mouse model of A beta deposition, *J*  
530 *Neuroinflamm*, 11 (2014).

531 [43] L.M. Tai, S. Ghura, K.P. Koster, V. Liakaite, M. Maienschein-Cline, P. Kanabar, N.  
532 Collins, M. Ben-Aissa, A.Z. Lei, N. Bahroos, S.J. Green, B. Hendrickson, L.J. Van Eldik,  
533 M.J. LaDu, APOE-modulated A beta-induced neuroinflammation in Alzheimer's disease:  
534 current landscape, novel data, and future perspective, *J Neurochem*, 133 (2015) 465-488.

535 [44] S. Utter, I.Y. Tamboli, J. Walter, A.R. Upadhaya, G. Birkenmeier, C.U. Pietrzik, E.  
536 Ghebremedhin, D.R. Thal, Cerebral small vessel disease-induced apolipoprotein E leakage is  
537 associated with Alzheimer disease and the accumulation of amyloid beta-protein in  
538 perivascular astrocytes, *J Neuropath Exp Neur*, 67 (2008) 842-856.

539 [45] D. Boche, C. Holmes, D. Wilkinson, V. Hopkins, A. Bayer, R. Jones, R. Bullock, S.  
540 Love, J. Neal, G. Yadegarfar, E. Zotova, J.A.R. Nicoll, Continued progression of  
541 neurodegeneration in Alzheimer's disease despite complete removal of the A beta plaques?,  
542 *Neuropath Appl Neuro*, 34 (2008) 1-1.

- 543 [46] K. Sakai, D. Boche, R. Carare, D. Johnston, C. Holmes, S. Love, J.A.R. Nicoll, A beta  
544 immunotherapy for Alzheimer's disease: effects on apoE and cerebral vasculopathy, *Acta*  
545 *Neuropathol*, 128 (2014) 777-789.
- 546 [47] D.J. Werring, R. Sperling, Inflammatory cerebral amyloid angiopathy and amyloid-  
547 modifying therapies: Variations on the Same ARIA?, *Ann Neurol*, 73 (2013) 439-441.